PAPER

Check for updates

Wet flue gas CO_2 capture and utilization using one-dimensional metal–organic chains†

Nan Chieh Chiu, [ID] [a] Ryan P. Loughran, [ID] [a] Andrzej Gładysiak,[b]
Rebecca Vismara, [ID] [c] Ah-Hyung Alissa Park [ID] [b] and Kyriakos C. Stylianou [ID] *[a]

Herein, we describe the use of an ultramicroporous metal–organic framework (MOF) with a composition of $[Ni_3(pzdc)_2(ade)_2(H_2O)_{1.5}] \cdot (H_2O)_{1.3}$ (pzdc: 3,5-pyrazole dicarboxylic acid; ade: adenine), for the selective capture of carbon dioxide (CO_2) from wet flue gas followed by its conversion to value-added products. This MOF is comprised of one-dimensional Ni(II)-pyrazole dicarboxylate-adenine chains; through pi–pi stacking and H-bonding interactions, these one-dimensional chains stack into a three-dimensional supramolecular structure with a one-dimensional pore network. Upon heating, our MOF undergoes a color change from light blue to lavender, indicating a change in the coordination geometry of Ni(II). Variable temperature ultraviolet-visible (UV/vis) spectroscopy data revealed a blue shift of the d–d transitions, suggesting a change in the Ni-coordination geometry from octahedral to a mixture of square planar and square pyramidal. The removal of the water molecules coordinated to Ni(II) leads to the generation of a MOF with open Ni(II) sites. Nitrogen isotherms collected at 77 K and 1 bar revealed that this MOF is microporous with a pore volume of 0.130 cm^3 g^{-1}. Carbon dioxide isotherms show a step in the uptake at low pressure, after which the CO_2 uptake is saturated. The step in the CO_2 uptake is likely attributable to the rearrangement of the three-dimensional supramolecular structure to accommodate CO_2 within its pores. The affinity of this MOF for CO_2 is 35.5 kJ mol^{-1} at low loadings, and it increases to 41.9 kJ mol^{-1} at high loadings. While our MOF is porous to CO_2 and water (H_2O) at 298 K, it is not porous to N_2, and the CO_2/ N_2 selectivity increases from 28.5 to 31.5 as a function of pressure. Breakthrough experiments reveal that this MOF can capture CO_2 from dry and wet flue gas with uptake capacities of 1.48 ± 0.01 and 1.14 ± 0.06 mmol g^{-1}, respectively. The MOF can be regenerated and reused at least three times, demonstrating consistent CO_2 uptake capacities. Upon understanding the sorption behavior of this MOF, catalysis experiments show that the MOF is catalytically active in the fixation of CO_2 into an epoxide ring for the formation of a cyclic carbonate. The turnover frequency for this reaction is 21.95 ± 0.03 h^{-1}. The MOF showed no catalytic deterioration after two cycles and maintained comparable catalytic activity when dry and wet CO_2/N_2 mixtures were used. This highlights that both N_2 and H_2O do not dramatically affect the catalytic activity of our MOF toward CO_2 fixation.

Introduction

The climate crisis threatening the world is being fueled by exorbitant volumes of CO_2 in the atmosphere.[1,2] As the accumulation of this greenhouse gas continues, global leaders

have recognized the need for curbing emissions, agreeing to an ambitious goal to cut emissions by 50% by 2030 in the 2015 Paris Climate Agreement.[3] Even though private companies work towards direct capture of CO_2 from the air,[4] we have yet to develop a sufficient mitigation strategy to scrub CO_2 from the waste gases produced from the combustion of fossil fuels and coal. In order to meet the goals set by world leaders, there is a clear impetus for new strategies toward environmental remediation. While the capture of CO_2 is undoubtedly a requirement in averting a climate catastrophe, the storage thereof is a topic of debate. Experts recommend storing captured CO_2 in caverns deep underground, while others recommend pumping CO_2 to the deep ocean floor to form CO_2 lakes.[5] Storage methods have merits, but ultimately their implementation will be governed by a cost-benefit analysis;

[a]*Materials Discovery Laboratory (MaD Lab), Department of Chemistry, Oregon State University, Corvallis, Oregon, USA. E-mail: kyriakos.stylianou@oregonstate.edu*
[b]*Department of Earth and Environmental Engineering, Department of Chemical Engineering, Lenfest Center for Sustainable Energy, Columbia University, New York, USA*
[c]*Departamento de Química Inorgánica, Universidad de Granada, 18071 Granada, Spain*

spending money to pump CO_2 into a limited number of underground caverns may not be seen as economically prudent in the long term. A preferable strategy is to capture CO_2 followed by its valorization to form value-added products.[1,6] This strategy of carbon capture and utilization (CCU) requires strong host–guest interactions, between adsorbents and CO_2, for efficient capture of CO_2 followed by its recycling for further usage. Through CCU, CO_2 emissions will not only be reduced, but it will be possible to produce molecules of added value using CO_2 as a feedstock.

Among the many adsorbents and catalysts that have been tested for CCU, metal–organic frameworks (MOFs) have shown great potential. MOFs are a class of crystalline materials boasting exceptionally high porosity, pore-volume, and tunability.[7,8] Their use as adsorbents toward pure CO_2 is well described in the literature,[1,9–13] but their use under industrially relevant conditions remains somewhat unexplored. Stability in water and high selectivity for CO_2 over N_2 are imperative in material design, as the most prolific source of CO_2 emissions is post-combustion flue gas (PCFG), such as that given off through combustion of coal.[7] PCFG is comprised of approximately 75% N_2, 15% CO_2, and 5–7% H_2O, with other gases present in low concentrations. Therefore, to capture CO_2 from PCFG, an effective material must demonstrate high uptake of CO_2 at 150 mbar pressure under simulated flue gas conditions while simultaneously demonstrating selectivity for CO_2 over the primary competing gases, N_2 and H_2O. Many of the best-performing MOFs to date are limited in their use by the presence of water.[14–16] The two functionalities that grant the highest CO_2 affinity are Lewis acidic open metal sites and Lewis basic amine groups.[17–19] Open metal sites will form dative bonds with electrons from the O atom of CO_2, while Lewis bases will perform a nucleophilic attack on the C atom of CO_2 to form carbamate compounds. However, these sites cannot typically be used in the presence of water, as water can either bind more strongly than CO_2 or can hydrolyze the metal–organic bonds, collapsing the MOF. For example, Mg-MOF-74, with open Mg(II) sites, demonstrates exceptionally high CO_2 uptake —reported at 5.28 mmol g^{-1}—but after exposure to 70% relative humidity (RH), the uptake drops by 84%, and its surface area decreases from 1800 m^2 g^{-1} to just 6 m^2 g^{-1}.[20,21] The porphyrin-based framework Al-PMOF has hydrophobic pores, which grants it resilience in the presence of water; it was designed to form a "perfect pocket" for CO_2 uptake by spacing the porphyrin rings apart by ∼7 Å. As such, Al-PMOF suffers no dramatic loss in CO_2 capture capacity under wet flue gas conditions.[2] Due to its stability and resilience to water, Al-PMOF represents a prime example of material design that should be explored as we continue to search for a functional CO_2 adsorbent in the presence of water. However, the CO_2 uptake capacity of Al-PMOF is low, and therefore we must continue developing new MOF designs to further improve their uptake under humid conditions.[2] Table 1 summarizes the characteristics of some common MOFs reported for CO_2 capture, as well as other non-MOF materials. It can be seen that our MOF demonstrates comparable uptake to the similarly-pillared structure of IISERP-MOF2,[22] though the pillared ZnAtzOx[23] and CALF-20[24] still perform better. Compared to inorganic/organic MOF hybrids like NbOFFIVE-1-Ni and TIFSIX-3-Ni,[25] our MOF uptakes about twice the amount of CO_2 at 150 mbar. Traditional benchmarks, like Mg-MOF-74,[26] UTSA-16,[27] and Zeolite 13X[26] boast exceptionally high CO_2 uptake compared to our material, but suffer tremendous performance attenuation after exposure to humidity.

In addition to the selective capture of CO_2 by MOFs, CO_2 conversion represents an opportunity for governments and private companies to recoup, over time, costs associated with installing and operating carbon-capture systems. Propylene carbonate (PC) is synthesized through the catalytic fixation of CO_2 onto propylene oxide (PO). PC is used in organic and pharmaceutical reactions as a polar, aprotic solvent. It has been used as an electrolyte in lithium-ion batteries and in cosmetics, adhesives, and plastic products.[28,29] This conversion requires strong interactions between the host material and the epoxide ring and CO_2 capture within the pores of the MOF to promote efficient catalysis.[30] Additionally, the material should retain its catalytic efficiency over several cycles, as long-lived materials will ultimately be more profitable.

Table 1 Comparison of MOFs for carbon capture using static single CO_2 isotherms and under humid conditions

Adsorbent	Uptake at 150 mbar using CO_2 isotherms at 298 K (mmol g^{-1})	Selectivity for CO_2 over N_2 at low loading	Q_{st} towards CO_2 at low loading (kJ mol^{-1})	CO_2 uptake performance under humid conditions	Ref.
$[Ni_3(pzdc)_2(ade)_2]\cdot(H_2O)_{0.4}$	1.45	30.25	35.5	∼23% loss at 75% RH	This work
Al-PMOF	1.1	Not reported	53	∼10% loss at 85% RH	2
IISERP-MOF2	1.60	1850	33	∼7% loss at 50% RH	22
ZnAtzOx	2.7	240	40	6% loss after boiling in water 24 h	23
CALF-20	2.60	230	39	∼40% loss at 40% RH	24
NbOFFIVE-1-Ni	0.759	0.91 (CO_2/H_2O)	50	15% loss at 75% RH	25
TIFSIX-3-Ni	0.714	0.87 (CO_2/H_2O)	55	17% loss at 75% RH	25
Mg-MOF-74	5.28	65	45	84% loss at 70% RH	26
UTSA-16	2.37	314.7	34.6	Unknown; material stability not affected by moisture	27
Zeolite 13X	4.5	86	50	∼100% loss at 75% RH	26
SGU-29	0.922	3515	51	No loss at 90% RH	35

MOFs with Lewis acidic open metal sites, like HKUST-1 and Mg-MOF-74, can interact strongly with the O atom of the epoxide or CO_2, granting high PO and CO_2 affinity and therefore, catalytic activity.[31] These MOFs, however, have a tendency to collapse in the presence of water, limiting their use in the conversion of CO_2 under humid conditions. Our previously reported lanthanide MOF, Ce-HTCPB, offered open metal sites and resilience under humid PCFG conditions, but its CO_2 uptake was very low, which limits the rate of CO_2 fixation in the epoxide ring.[30] Therefore, the discovery of materials that can retain their CO_2 uptake capacity under humid conditions and be catalytically active in the fixation of CO_2 into PO for the production of PC is of great importance for the reduction of CO_2 emissions while useful materials can be produced.

Herein, we present a MOF with the formula $[Ni_3(pzdc)_2(ade)_2(H_2O)_4]\cdot(H_2O)_{1.3}$ (pzdc: 3,5-pyrazole dicarboxylic acid; ade: adenine) for dry and wet flue gas separation and CO_2 conversion into value added products. This MOF has been previously utilized for biogas and hydrocarbon separation.[13,32] The three-dimensional supramolecular structure of the MOF is uniquely comprised of stacked one-dimensional Ni-pyrazole dicarboxylate-adenine chains (Fig. 1). The coordination geometry of the Ni(II) sites in our MOF changes upon activation, leading to a color change from light blue to lavender. The removal of the water molecules coordinated to Ni(II) leads to the generation of a MOF with open Ni(II) sites. Our MOF is microporous, with a pore volume of 0.130 $cm^3\ g^{-1}$, but a step in the CO_2 isotherm at low pressures suggests that structural rearrangements occur upon CO_2 loading (i.e., pore expansion). This is further supported by an increase in the affinity of this MOF for CO_2 as more gas permeates the material. Breakthrough curves reveal that our MOF demonstrates selectivity towards CO_2 over N_2 and H_2O and does not suffer a significant loss in CO_2 uptake under humid PCFG conditions. Further, our MOF can catalyze the cycloaddition of CO_2 onto PO to form value-added PC and maintains its efficiency across multiple cycles and in the presence of water.

Results and discussion

Synthesis and solid-state characterization

The reaction of $NiCO_3$, adenine, and 3,5-pyrazole dicarboxylic acid in deionized water produces a crystalline blue powder with a formula of $[Ni_3(pzdc)_2(ade)_2(H_2O)_4]\cdot(H_2O)_{1.3}$. The structure of $[Ni_3(pzdc)_2(ade)_2(H_2O)_4]\cdot(H_2O)_{1.3}$ consists of one-dimensional chains containing two distinct Ni^{2+} (Ni_A and Ni_B), both in an octahedral geometry (Fig. 1). Adenine provides bidentate coordination to two adjacent Ni_A centers (formation of a Ni-dimer) via its pyrimidinate and imidazolate N atoms. The coordination environment of Ni_A is completed with a pyrazolate N atom, two carboxylate O atoms from pzdc ligands, and one water molecule. Ni_B is coordinated to two adjacent pzdc ligands from their pyrazolate N and carboxylate O atoms. Two water molecules in axial positions complete the coordination environment of Ni_B (Fig. 1). Adjacent one-dimensional chains are interlinked by π–π stacking and hydrogen bonding interactions between the adenine molecules. This results in the generation of a three-dimensional supramolecular and porous structure. Guest and bound water molecules can be removed following the activation of the material at 100 °C under vacuum (10^{-4} mbar). Successful activation of $[Ni_3(pzdc)_2(ade)_2(H_2O)_4]\cdot(H_2O)_{1.3}$ to $[Ni_3(pzdc)_2(ade)_2]\cdot(H_2O)_{0.4}$ can be confirmed by a color change of the powder from light blue to lavender (Fig. 2), and $[Ni_3(pzdc)_2(ade)_2]\cdot(H_2O)_{0.4}$ features one-dimensional porosity running along the a-axis. The pores in $[Ni_3(pzdc)_2(ade)_2]\cdot(H_2O)_{0.4}$, with dimensions of ~4.1 Å,[13,32] are functionalized with pyrimidinate, imidazolate, and pyrazolate N atoms and open Ni sites (Ni_A: square pyramidal and Ni_B: square planar geometries) which are ideal for carbon capture and utilization.

The bulk phase and analytical purity of $[Ni_3(pzdc)_2(ade)_2(H_2O)_4]\cdot(H_2O)_{1.3}$ was confirmed by powder X-ray diffraction (PXRD), Fourier transform infrared spectroscopy (FT-IR) and elemental analysis (EA). The PXRD pattern of the as-prepared material is in agreement with the
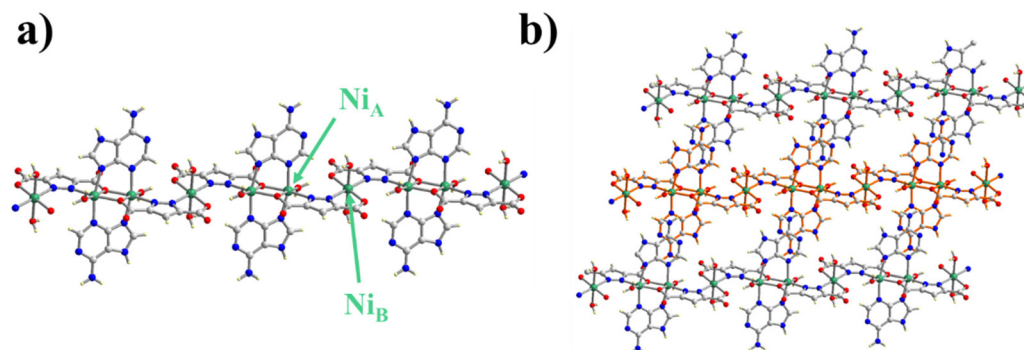
Fig. 1 Structural representation of $[Ni_3(pzdc)_2(ade)_2(H_2O)_4]\cdot(H_2O)_{1.3}$. (a) One-dimensional MOF chains are formed by Ni_A and Ni_B, 3,5-pyrazole dicarboxylate, and adenine ligands. The chains run along the crystallographic c axis. (b) Packing of the one-dimensional MOF chains results in the generation of a three-dimensional supramolecular structure. The one-dimensional chains with orange bonds reveal that pi–pi stacking and H-bonding interactions between adenine molecules in adjacent chains lead to the formation of one-dimensional pores running along the b axis. Atom color code: gray, carbon; red, oxygen; green, nickel; blue, nitrogen; pale yellow, hydrogen.
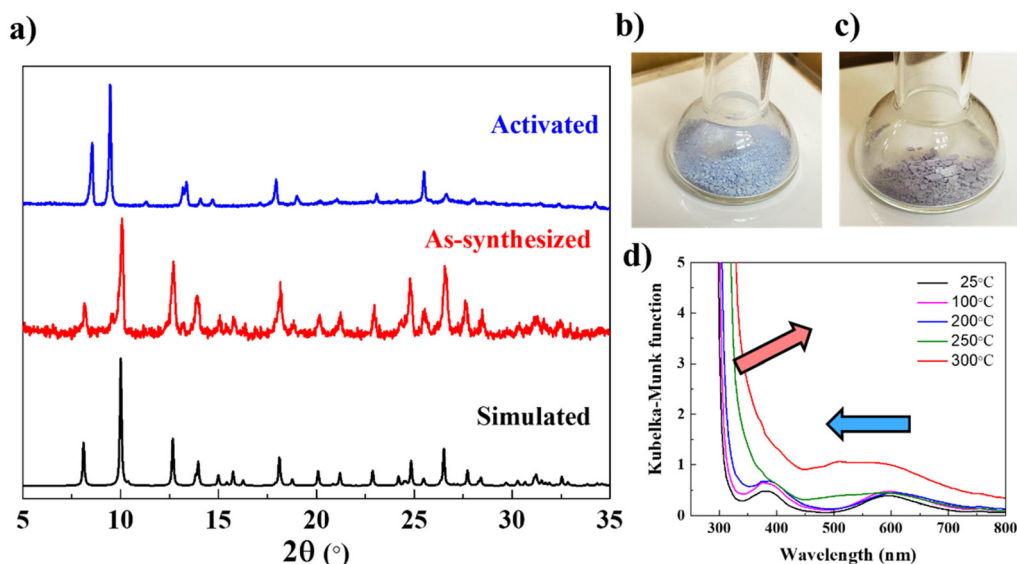
Fig. 2 (a) PXRD patterns of simulated (black), as-synthesized (red), and activated (blue) MOF. The agreement of simulated with as-synthesized patterns represented the purity of the as-synthesized $[Ni_3(pzdc)_2(ade)_2(H_2O)_4]\cdot(H_2O)_{1.3}$. The pattern for the dehydrated $[Ni_3(pzdc)_2(ade)_2]\cdot(H_2O)_{0.4}$ reveals that structural rearrangements may occur upon activation. Photos of the color of the MOF (b) before activation and (c) after activation. The color of the powder changed from blue to lavender after activation. (d) Temperature dependent Kubelka–Munk representation of diffuse reflectance spectra recorded from 25 °C to 300 °C. The absorption edge red-shifted from 25 °C (black), 100 °C (pink), 200 °C (blue), 250 °C (green), to 300 °C (red). The peak at 590 nm corresponds to d–d transitions. It began to blue-shift when the temperature reached 200 °C. This is attributed to the removal of bound water molecules to Ni and the coordination geometry change of Ni from octahedral to a mixture of square pyramidal and square planar.

corresponding simulated pattern (Fig. 2a). Importantly, this MOF is stable when immersed in liquid water for 24 h (Fig. S1†). The FT-IR spectrum of $[Ni_3(pzdc)_2(ade)_2(H_2O)_4]\cdot(H_2O)_{1.3}$ shows the disappearance of the N–H stretching band at 3350 cm^{-1}, which is present in the spectra of both adenine and pzdc ligands (Fig. S2†). This indicates successful deprotonation of the amines as the ligands bind to Ni^{2+} through their N atoms. Elemental analysis gives the composition of $[Ni_3(pzdc)_2(ade)_2(H_2O)_4]\cdot(H_2O)_{1.3}$ for the as-prepared material (Anal. Calcd: C 28.33, H 2.69, N 23.13; experimental: C 28.46, H 2.78, N 22.93). Thermogravimetric analysis (TGA) and temperature-dependent Kubelka–Munk analyses were used to probe the color and energetic shifts of the MOF upon activation. TGA showed that $[Ni_3(pzdc)_2(ade)_2(H_2O)_4]\cdot(H_2O)_{1.3}$ loses 8% of its mass at 170 °C, followed by another 4% loss at 260 °C (Fig. S3†). These mass losses are attributed to the removal of both guest and bound water molecules. The thermal degradation of the MOF starts at 365 °C. The temperature dependent Kubelka–Munk analysis was conducted from 25 to 300 °C (Fig. 2d). The absorbance spectrum of $[Ni_3(pzdc)_2(ade)_2(H_2O)_4]\cdot(H_2O)_{1.3}$ is shifted when the temperature was increased; this is thought to be due to the altered geometry of the Ni sites, as octahedrally coordinated Ni$_A$ and Ni$_B$ become square pyramidal and square planar when bound water molecules are removed.[33] The splitting of the d-orbitals results in the $d_{x^2-y^2}$ orbital losing an electron, and becoming unoccupied, which leads to a blue-shifted absorbance in the d–d transition region of the Kubelka–Munk analyses (*ca.* 590 → 550 nm). Hence, $[Ni_3(pzdc)_2(ade)_2]\cdot(H_2O)_{0.4}$ must absorb more light to excite

the electron to the $d_{x^2-y^2}$ orbital, so lower energy red light will be more heavily reflected, and the material thus shifts from light blue to light purple (lavender) in color. The PXRD pattern of the activated material (collected using a capillary packed in a glove box) is substantially different compared to the PXRD pattern of the as-prepared MOF, suggesting that structural rearrangements occur upon removal of the guest and bound water molecules (Fig. 2a). Notably, when the activated MOF (lavender color) is exposed to the atmosphere, the blue color of the hydrated MOF is recovered (Fig. 2b and c). This is attributed to the coordination of water molecules with Ni$_A$ and Ni$_B$, regenerating their octahedral geometries, and therefore the structure of $[Ni_3(pzdc)_2(ade)_2(H_2O)_4]\cdot(H_2O)_{1.3}$. Elemental analysis of the activated material revealed a formula of $[Ni_3(pzdc)_2(ade)_2]\cdot(H_2O)_{0.4}$ (Anal. Calcd: C 31.62, H 1.70, N 25.81; experimental: C 31.43, H 1.81, N 25.78). The water content in the activated material is thought to be due to the MOF's re-adsorption of water from the atmosphere.[13]

Single component isotherms

The permanent microporosity of the activated MOF was demonstrated by a Type I N$_2$ isotherm recorded at 77 K and 1 bar, following activation at 373 K under vacuum for 8 h (Fig. S4†). The Brunauer–Emmett–Teller (BET) surface area was calculated to be 183 m^2 g^{-1} (p/p^0 = 0.10–0.26). The pore volume of $[Ni_3(pzdc)_2(ade)_2]\cdot(H_2O)_{0.4}$ was calculated using N$_2$ uptake at 77 K and 1 bar, which is 0.130 cm^3 g^{-1}. Volumetric CO$_2$ isotherms on the activated MOF were collected at 293, 298, and 303 K at 1 bar (Fig. 3a and S5†). The MOF was stable
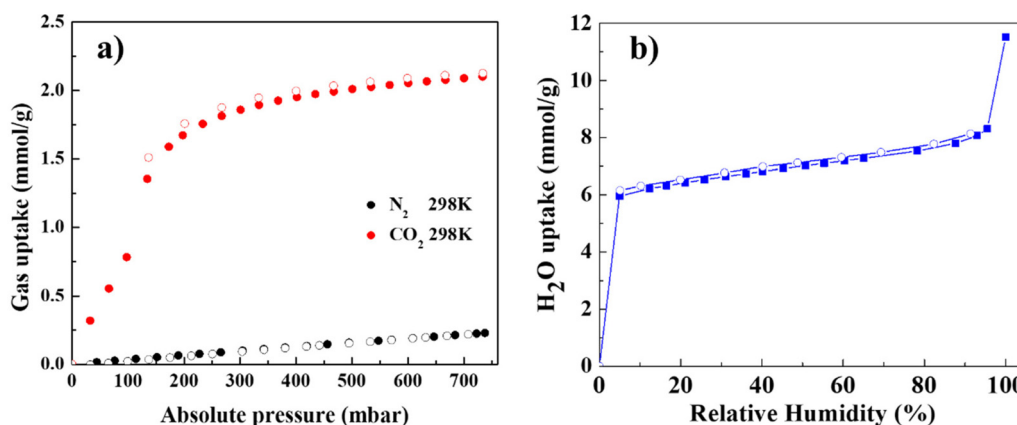
Fig. 3 (a) Comparison of N_2 and CO_2 isotherms collected on the activated $[Ni_3(pzdc)_2(ade)_2]\cdot(H_2O)_{0.4}$ at 298 K. $[Ni_3(pzdc)_2(ade)_2]\cdot(H_2O)_{0.4}$ showed higher uptakes of CO_2 (red) compared to N_2 (black). (b) Water isotherm collected at 298 K.

after CO_2 isotherm analysis which was confirmed by the PXRD results (Fig. S6†). The CO_2 isotherms are all reversible, but unlike other microporous MOFs,[7,12,34] we observed that these isotherms show a weak step; this stepped CO_2 uptake indicates structural rearrangements upon diffusion of CO_2 in the pores of the activated MOF. We hypothesize that upon activation, the MOF pores, although accessible to CO_2, are slightly smaller compared to the size of CO_2. However, due to the unique stacking arrangement of the one-dimensional MOF chains, the chains can rearrange to open the pore wider, allowing the CO_2 to be fixed in the pores upon further loading. This step is observed for all CO_2 isotherms recorded at 293, 298, and 303 K, and importantly the CO_2 uptake at 1 bar was found to be approximately 2.1–2.2 mmol g^{-1} for all three temperatures (Fig. S5†). At 298 K, the CO_2 uptake at 150 mbar is 1.45 mmol g^{-1}. Isosteric heats of adsorption (Q_{st}) were calculated using the Clausius–Clapeyron equation using the adsorption branches obtained at 273, 298 and 303 K. We found that the binding enthalpy increases as a function of CO_2 loading: at low pressure, the Q_{st} was calculated to be 35.5 kJ mol^{-1}, and at high CO_2 loading, the Q_{st} increased to 41.9 kJ mol^{-1} (Fig. S7†). These values are comparable to other large pore and functional materials such as Al-PMOF,[2] Al-PyrMOF,[2] CALF-20,[24] and SGU-29,[35] but lower than MOFs with amine-functionalized pores like the mmen-Mg_2(dobpdc).[36]

$[Ni_3(pzdc)_2(ade)_2]\cdot(H_2O)_{0.4}$ showed low N_2 uptake at 298 K, 0.22 mmol g^{-1} at 0.76 bar (Fig. 3a). The higher uptake observed for CO_2 over N_2 is thought to be due to the pore size and functionality, which is decorated with open Ni(II) metal sites and Lewis basic adenine- and pyrazolate-N atoms. The selectivity of CO_2 over N_2 was further analyzed by employing ideal adsorbed solution theory (IAST) which models mixed-gas adsorption isotherms based on the single-component adsorption isotherms.[37] As shown in Fig. S8,† $[Ni_3(pzdc)_2(ade)_2]\cdot(H_2O)_{0.4}$ demonstrates selectivity ranging from 28.5 to 31.5 and CO_2/N_2 selectivity between 10 and 400 mbar. The selectivity of the MOF to CO_2 over N_2 is attributed to Lewis acid/base interactions between the open metal sites of the MOF and the lone pairs of either gas molecule. CO_2 is more polarizable than N_2 (26.3×10^{-25} cm^3 *vs.* 17.6×10^{-25} cm^3, respectively), which means the electrons can be pulled more strongly towards the CO_2 oxygen than the N_2 nitrogen, making CO_2 a stronger Lewis base.

Additionally, the quadrupole moment of CO_2 is higher than that of N_2 (13.4×10^{-40} C m^2 *vs.* 4.7×10^{-40} C m^2, respectively), which means that there is a greater difference in electron distribution throughout the CO_2 molecule than the N_2 molecule, which can lead to interactions between captured CO_2 and free CO_2 to further increase uptake beyond the Lewis interactions within the pore.[38] Given the Lewis acidic open nickel sites within the pores, as well as the Lewis basic nitrogen atoms in the ligands, there are stronger interactions with CO_2 molecules than N_2, affording selectivity for the target molecules.

The water isotherm recorded at 298 K indicates that $[Ni_3(pzdc)_2(ade)_2]\cdot(H_2O)_{0.4}$ uptakes 11.5 mmol g^{-1} at 100% humidity (~30 mbar) (Fig. 3b). The steep water uptake at low relative humidity (%RH) is supported by the color change of the activated material when it is exposed to air: the lavender color turns blue as water molecules begin to occupy the open metal sites.

The hydrolytic and thermal stability of this MOF, pore size, and functionalization, as well as its high affinity and selectivity for CO_2 over N_2, prompted us to study the selective capture of CO_2 from simulated dry and wet flue gas compositions: 15 : 85 CO_2/N_2 and 15 : 85 CO_2/N_2 at 75% relative humidity.

Breakthrough curves for CO_2 under dry and humid conditions

Breakthrough experiments were performed to evaluate the separation performance of $[Ni_3(pzdc)_2(ade)_2]\cdot(H_2O)_{0.4}$ under dry and wet flue gas streams at 298 K (Fig. 4, S9, and S10†). For these experiments, $[Ni_3(pzdc)_2(ade)_2(H_2O)_4]\cdot(H_2O)_{1.3}$ was first packed into columns of a fixed bed reactor, followed by its activation at 110 °C. A dilute CO_2 stream (15 vol% CO_2 and 85% of N_2, mimicking PCFG conditions)[7] was then introduced into the column, and the CO_2 uptake capacities of our MOF were determined. After each experiment, the material was regener-
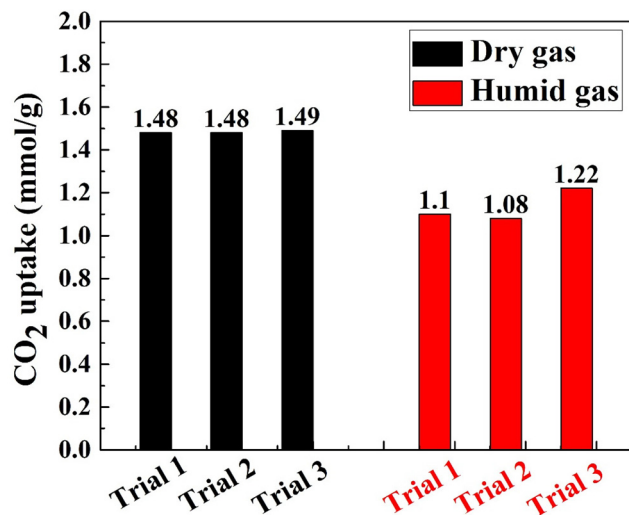
Fig. 4 Comparison of the CO_2 uptakes collected on a column packed with $[Ni_3(pzdc)_2(ade)_2] \cdot (H_2O)_{0.4}$ under dry (CO_2/N_2, 85/15) and humid (CO_2/N_2 under RH, 85/15 under 75RH) conditions at 298 K. Trials 2 and 3 reveal that the MOF can be successfully regenerated and shows consistent uptakes for each trial.

ated through temperature swing, and its separation performance was tested three times. For experiments under wet conditions, the gas stream was humidified up to 75% RH using a gas sparger prior to introduction into the reactor. Under dry conditions, the CO_2 capacity of our MOF was 1.48 ± 0.01 mmol g^{-1} (Fig. 4). The CO_2 dynamic breakthrough capacity was comparable to the uptake derived from the static single gas adsorption isotherm collected under the same temperature and CO_2 partial pressure (150 mbar). This indicates that our MOF was fully activated, and N_2 has no impact on the capture of CO_2. Under humid conditions, the CO_2 uptake capacity was slightly lower at 1.14 ± 0.06 mmol g^{-1} (Fig. 4); this is thought to be due to the competition between CO_2 and H_2O within the pores of $[Ni_3(pzdc)_2(ade)_2] \cdot (H_2O)_{0.4}$. After the pores are saturated with CO_2, we see that water vapors slowly start to displace some of the adsorbed CO_2 (Fig. S9 and S10†). Importantly, despite the high affinity of our activated MOF for water, breakthrough analyses show that CO_2 is adsorbed first from a humid PCFG mixture, demonstrating consistent CO_2 uptakes for at least three cycles.

The adsorbents described in Table 1 represent some of the only solid-state CO_2 adsorbents with performance measured in the presence of humidity. Their CO_2 uptake nearly always suffers in the presence of water, with the exception of copper silicate SGU-29,[35] but this is an important metric that should not be disregarded, as all sources of post-combustion flue gas have varying levels of humidity. Common benchmarks like Mg-MOF-74 cannot be implemented directly for CO_2 capture under such conditions and still maintain the uptake they demonstrate from single-component CO_2 isotherms, because flue gas is not a single-component gas. When determining the validity of a CO_2 adsorbent, it is important to consider not only the uptake, but also the performance in the presence of water. In this regard, our material's performance retention in

the presence of 75% RH allows it to match or exceed the performance of all other materials with higher single-component uptake.

CO_2 fixation onto an epoxide for the formation of cyclic carbonate

The activated MOF exhibits a high affinity for CO_2, as well as selectivity for CO_2 over N_2 and H_2O, because the combination of open Lewis acid sites and Lewis bases decorate the pores of the MOF. The strength of the host–guest interactions allowed us to test the catalytic activity of this MOF for the fixation of CO_2 onto PO for the formation of PC. The proposed mechanism first requires the epoxide to coordinate with one of the Lewis acidic Ni(II) sites, where nucleophilic tetrabutylammonium bromide (TBAB) can catalyze the opening of the epoxide ring. The ring-opening generates a carbocation in the epoxide, which reacts spontaneously with the nucleophilic O atom from CO_2. The C atom of CO_2 then becomes electrophilic and reacts with the O atom of the epoxide, closing the ring and yielding PC.[30] The accessibility and density of open sites are vital for enhancing the turnover frequency (TOF) of the cycloaddition reaction. Hence, we hypothesized that our MOF could potentially serve as a catalyst in the cycloaddition of CO_2 onto epoxides. The cycloaddition reaction was conducted by mixing our three-dimensional supramolecular MOF with the solution, including PO, TBAB, and 1,2-dimethoxyethane (DME). TBAB acted as the co-catalyst that provided the nucleophilic Br^- for promoting the ring-opening. The suspension was transferred to the stainless-steel Parr reactor, which was pressurized to 10 bar with CO_2 and heated at 100 °C for 1, 2, and 4 h. ^1H-NMR was used to analyze and calculate the yield of propylene carbonate (PC) after the reaction (see the ESI for details and Fig. S11†). As can be seen in Fig. 5, our MOF successfully converted CO_2 and PO into PC at relatively low reaction times. For 1 h and 2 h reactions, we observed a 49.22% and 53.12% yield with TOF values of 50.93 h^{-1} and 27.49 h^{-1}, respectively. The 4 h reaction time reached the highest yield of 84.94 ± 0.01%, with a TOF of 21.95 ± 0.03 h^{-1}. After the reaction was finished, this MOF was washed with DI water and dried for the cycle test. The second cycle of this reaction showed a TOF of 21.92 ± 0.06 h^{-1}, which was comparable to the result we observed in the first cycle (Fig. 5). Moreover, the PXRD pattern of the MOF after catalysis showed a similar pattern to that before catalysis, confirming its stability (Fig. S12†). For the same reaction catalyzed by our aforementioned MOF, Ce-HTCPB, we reported a TOF of 20.2 ± 0.26 h^{-1}.[30] The catalytic efficiency of our MOF is greater, by comparison, largely owing to its pore functionality.

While this catalytic reaction is well studied, there are only a few works describing the activity of catalysts in dry and wet CO_2/N_2 mixtures, including the ZnGlu and ZSF-1.[39,40] To probe the effects of competing gases, a catalytic reaction was performed with a 50 : 50 CO_2/N_2 gas mixture at 20 bar (10 bar CO_2 and 10 bar N_2) at 100 °C for 4 h. Due to the high selectivity of CO_2 over N_2, we could still convert PO and CO_2 to PC with a 75.15% yield and a TOF of 19.44 h^{-1}. Furthermore, a catalytic
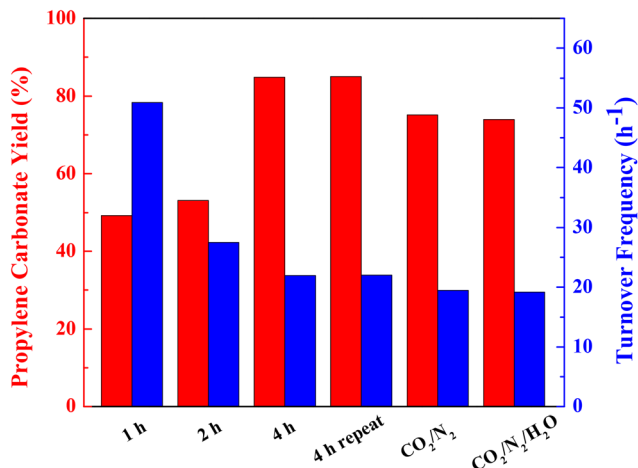
Fig. 5 Comparison of conversion yield and TOF of the CO_2 fixation onto PO to PC for $[Ni_3(pzdc)_2(ade)_2(H_2O)_4]\cdot(H_2O)_{1.3}$ at 100 °C and 10 bar of pure CO_2. From left to right: 1 h reaction time, 2 h reaction time, 4 h reaction time, regeneration and reuse − 4 h reaction time, with 50 : 50 CO_2/N_2 gas mixture (20 bar), with 50 : 50 CO_2/N_2 gas mixture (20 bar) in the presence of water.

reaction was conducted under aqueous conditions with mixed gases to investigate the competing effect of water. A mixture of DME/DI-water in a ratio of 9 : 1 was used as the solvent for the catalytic reaction with a 50 : 50 CO_2/N_2 gas mixture at 20 bar (10 bar CO_2 and 10 bar N_2) at 100 °C for 4 h. PC was produced with a 73.95% conversion yield and TOF of 19.13 h^{-1} (Fig. 5). This was similar to the moisture-free gas mixture catalytic reaction. We believe that the presence of water showed a minimum effect on the catalytic reaction since $[Ni_3(pzdc)_2(ade)_2(H_2O)_4]\cdot$ $(H_2O)_{1.3}$ is water-stable and has a higher affinity for CO_2 over N_2 and H_2O, as supported by the breakthrough curves of the MOF under humid conditions. Table S1† provides a comparison of our material to other catalysts reported for the same reaction. After only 4 hours, our material boasted nearly an 85% yield and a TOF of 21.95 h^{-1}. In previous work, we demonstrated a comparable TOF under the same conditions with [Ce(HTCPB)] and NH$_2$-MIL-101(Al), but these MOFs required 12 and 6 hours, respectively, to reach >95% yield.

Conclusion

To summarize, we have shown that the unique packing of the one-dimensional chains of $[Ni_3(pzdc)_2(ade)_2(H_2O)_4]\cdot(H_2O)_{1.3}$ leads to the generation of a three-dimensional porous framework that exhibits a high affinity for CO_2 and selectivity for CO_2 over N_2. Its sorption behavior is attributed to an interplay of pore size and functionality as well as the presence of both Lewis acidic open metal sites and Lewis basic N atoms decorating the pores. As a result, upon activation, the MOF can selectively capture CO_2 under dry, and flue gas streams with consistent uptakes for at least three cycles. We also demonstrate that this MOF is catalytically active for the fixation of CO_2 onto an epoxide ring for the production of a cyclic carbonate. We

found that this MOF can catalyze this reaction when pure or diluted CO_2 streams are used. This work shows that MOFs can play an important role in mitigating the climate crisis. While many proposed solutions would seek to deposit captured CO_2 deep below the surface, $[Ni_3(pzdc)_2(ade)_2(H_2O)_4]\cdot(H_2O)_{1.3}$ offers a more economically viable alternative by capturing and revalorizing CO_2 to the valuable propylene carbonate.

Data availability statement

The data supporting this study's findings are available in the ESI of this article.†

Author contributions

K. C. S. conceived the project and designed the experiments together with N. C. C. N. C. C. led the experiments and, together with R. P. L., interpreted the data. A. G. and A.-H. A. P. performed the breakthrough experiments and calculated the CO_2 capacity under dry and humid conditions. R. V. collected the water isotherms. K. C. S., N. C. C., and R. P. L. wrote the manuscript with contributions from all authors.

Conflicts of interest

The authors declare no competing interests.

Acknowledgements

References

1 J. W. Maina, C. Pozo-Gonzalo, L. Kong, J. Schütz, M. Hill and L. F. Dumée, *Mater. Horiz.*, 2017, **4**, 345–361.
2 P. G. Boyd, A. Chidambaram, E. García-Díez, C. P. Ireland, T. D. Daff, R. Bounds, A. Gładysiak, P. Schouwink, S. M. Moosavi, M. M. Maroto-Valer, J. A. Reimer, J. A. R. Navarro, T. K. Woo, S. Garcia, K. C. Stylianou and B. Smit, *Nature*, 2019, **576**, 253–256.
3 N. Glanemann, S. N. Willner and A. Levermann, *Nat. Commun.*, 2020, **11**, 110.
4 https://climeworks.com.
5 M. J. Bickle, *Nat. Geosci.*, 2009, **2**, 815–818.
6 C. Maeda, Y. Miyazaki and T. Ema, *Catal. Sci. Technol.*, 2014, **4**, 1482–1497.

7   K. Sumida, D. L. Rogow, J. A. Mason, T. M. McDonald, E. D. Bloch, Z. R. Herm, T.-H. Bae and J. R. Long, *Chem. Rev.*, 2012, **112**, 724–781.

8   M. Ding, R. W. Flaig, H.-L. Jiang and O. M. Yaghi, *Chem. Soc. Rev.*, 2019, **48**, 2783–2828.

9   Y. Huang, S. Zhang, H. Chen, L. Zhao, Z. Zhang, P. Cheng and Y. Chen, *Inorg. Chem.*, 2019, **58**, 9916–9921.

10 C. E. Bien, Q. Liu and C. R. Wade, *Chem. Mater.*, 2020, **32**, 489–497.

11 C. E. Bien, K. K. Chen, S.-C. Chien, B. R. Reiner, L.-C. Lin, C. R. Wade and W. S. W. Ho, *J. Am. Chem. Soc.*, 2018, **140**, 12662–12666.

12 A. Gładysiak, K. S. Deeg, I. Dovgaliuk, A. Chidambaram, K. Ordiz, P. G. Boyd, S. M. Moosavi, D. Ongari, J. A. R. Navarro, B. Smit and K. C. Stylianou, *ACS Appl. Mater. Interfaces*, 2018, **10**, 36144–36156.

13 K. C. Stylianou, J. E. Warren, S. Y. Chong, J. Rabone, J. Bacsa, D. Bradshaw and M. J. Rosseinsky, *Chem. Commun.*, 2011, **47**, 3389–3391.

14 D.-A. Yang, H.-Y. Cho, J. Kim, S.-T. Yang and W.-S. Ahn, *Energy Environ. Sci.*, 2012, **5**, 6465–6473.

15 N. Vrtovec, M. Mazaj, G. Buscarino, A. Terracina, S. Agnello, I. Arčon, J. Kovač and N. Zabukovec Logar, *Cryst. Growth Des.*, 2020, **20**, 5455–5465.

16 M. T. Kapelewski, S. J. Geier, M. R. Hudson, D. Stück, J. A. Mason, J. N. Nelson, D. J. Xiao, Z. Hulvey, E. Gilmour, S. A. FitzGerald, M. Head-Gordon, C. M. Brown and J. R. Long, *J. Am. Chem. Soc.*, 2014, **136**, 12119–12129.

17 R. A. Agarwal and D. De, *Polyhedron*, 2020, **185**, 114584.

18 A. K. Gupta, N. Guha, S. Krishnan, P. Mathur and D. K. Rai, *J. CO2 Util.*, 2020, **39**, 101173.

19 J. Gu, X. Sun, X. Liu, Y. Yuan, H. Shan and Y. Liu, *Inorg. Chem. Front.*, 2020, **7**, 4517–4526.

20 A. A. Voskanyan, V. G. Goncharov, N. Novendra, X. Guo and A. Navrotsky, *ACS Omega*, 2020, **5**, 13158–13163.

21 J. Yu, L.-H. Xie, J.-R. Li, Y. Ma, J. M. Seminario and P. B. Balbuena, *Chem. Rev.*, 2017, **117**, 9674–9754.

22 S. Nandi, S. Collins, D. Chakraborty, D. Banerjee, P. K. Thallapally, T. K. Woo and R. Vaidhyanathan, *J. Am. Chem. Soc.*, 2017, **139**, 1734–1737.

23 A. Banerjee, S. Nandi, P. Nasa and R. Vaidhyanathan, *Chem. Commun.*, 2016, **52**, 1851–1854.

24 J.-B. Lin, T. T. T. Nguyen, R. Vaidhyanathan, J. Burner, J. M. Taylor, H. Durekova, F. Akhtar, R. K. Mah, O. Ghaffari-Nik, S. Marx, N. Fylstra, S. S. Iremonger, K. W. Dawson, P. Sarkar, P. Hovington, A. Rajendran, T. K. Woo and G. K. H. Shimizu, *Science*, 2021, **374**, 1464–1469.

25 A. Kumar, C. Hua, D. G. Madden, D. O'Nolan, K.-J. Chen, L.-A. J. Keane, J. J. Perry and M. J. Zaworotko, *Chem. Commun.*, 2017, **53**, 5946–5949.

26 T. Remy, S. A. Peter, S. Van der Perre, P. Valvekens, D. E. De Vos, G. V. Baron and J. F. M. Denayer, *J. Phys. Chem. C*, 2013, **117**, 9301–9310.

27 S. Xiang, Y. He, Z. Zhang, H. Wu, W. Zhou, R. Krishna and B. Chen, *Nat. Commun.*, 2012, **3**, 954.

28 D. Stoye, in *Ullmann's Encyclopedia of Industrial Chemistry*, 2012, DOI: **10.1002/14356007.a24_437**.

29 M. Schroeder, M. Winter, S. Passerini and A. Balducci, *J. Electrochem. Soc.*, 2012, **159**, A1240–A1245.

30 D. H. Le, R. P. Loughan, A. Gładysiak, N. Rampal, I. A. Brooks, A.-H. A. Park, D. Fairen-Jimenez and K. C. Stylianou, *J. Mater. Chem. A*, 2022, **10**, 1442–1450.

31 S. G. Musa, Z. M. Aljunid Merican and O. Akbarzadeh, *Polymers*, 2021, **13**, 3905.

32 Z. Zhang, S. B. Peh, Y. Wang, C. Kang, W. Fan and D. Zhao, *Angew. Chem., Int. Ed.*, 2020, **59**, 18927–18932.

33 F. Giordanino, P. N. R. Vennestrøm, L. F. Lundegaard, F. N. Stappen, S. Mossin, P. Beato, S. Bordiga and C. Lamberti, *Dalton Trans.*, 2013, **42**, 12741–12761.

34 A. Chidambaram, D. H. Le, J. A. R. Navarro and K. C. Stylianou, *Appl. Mater. Today*, 2021, **22**, 100933.

35 S. J. Datta, C. Khumnoon, Z. H. Lee, W. K. Moon, S. Docao, T. H. Nguyen, I. C. Hwang, D. Moon, P. Oleynikov, O. Terasaki and K. B. Yoon, *Science*, 2015, **350**, 302–306.

36 T. M. McDonald, W. R. Lee, J. A. Mason, B. M. Wiers, C. S. Hong and J. R. Long, *J. Am. Chem. Soc.*, 2012, **134**, 7056–7065.

37 C. M. Simon, B. Smit and M. Haranczyk, *Comput. Phys. Commun.*, 2016, **200**, 364–380.

38 M. Oschatz and M. Antonietti, *Energy Environ. Sci.*, 2018, **11**, 57–70.

39 A. C. Kathalikkattil, R. Roshan, J. Tharun, R. Babu, G.-S. Jeong, D.-W. Kim, S. J. Cho and D.-W. Park, *Chem. Commun.*, 2016, **52**, 280–283.

40 J. Li, Y. Ren, C. Yue, Y. Fan, C. Qi and H. Jiang, *ACS Appl. Mater. Interfaces*, 2018, **10**, 36047–36057.